

# Incommensurable time intervals for multi-exposure PTV

Ilda Hysa<sup>1,2\*</sup>, Fulvio Scarano<sup>2</sup>, Andrea Sciacchitano<sup>2</sup>, Marthijn Tuinstra<sup>1</sup>

1: Vertical Flight and Aeroacoustics Department, Dutch Aerospace Center, Marknesse, Netherlands

2: Aerospace Engineering Faculty, Delft, Netherlands

\* Correspondent author: ilda.hysa@nlr.nl

**Keywords:** multiple-exposure, time-space scaling, trajectory identification, illumination pulse code tailoring

## ABSTRACT

A novel approach to the analysis of multiply exposed particle image recordings at low source density is presented. The foundation of the method is the similarity between the time sequence of multiple light pulses and the set of positions marked along the trajectory of a Lagrangian tracer. The study discusses the properties of the time sequence to obtain unambiguous identifications of the particles trajectories and directions of motion.

The identification of the particles trajectories from multi-exposed image recordings relies on the inner product between two signals, namely the time-sequence of the illumination pulses and the positions of the selected set of particle images. Considering double-frame image recordings, the origin of every track is set in the first frame, where the tracers are exposed a single time. Instead, in the second frame, the tracers are illuminated multiple times.

A scaling operation (homothety) based on the estimated track velocity is performed to express the two signals in the same domain, namely time. The inner product is repeated for different values of the estimated track velocity and the signal-to-noise ratio is taken as relevant parameter for robust track identification.

An ordinary sequence with regularly time separation between pulses suffers from a low signal-to-noise ratio because of the high probability of spurious matching. Instead, irregular and incommensurable intervals offer the highest signal-to-noise.

The concept is demonstrated with an experimental dataset based on high-speed recordings of the turbulent flow across a cylinder obstacle. Multiply-exposed recordings are simulated superimposing instantaneous recordings, where the choice of the time sequence could be varied finely. The method detects successfully particle tracks and assigns correctly the particles time stamp in approximately 80% of the domain. At very low velocity (<3% of free stream), the superposition of the particle images over several exposures hampers the detection of individual particle images.

---

## 1. Introduction

Historically, multiple-exposure (ME) PIV images were recorded on photographic film, and ME was needed due to the limited acquisition frequency, or frame rate, of the available cameras. The analysis of recordings featuring multiple exposures of particle tracers dates back to the early work

of Utami & Ueno (1984) who investigated the turbulent channel flow. The particle motion was coded with four pulses produced with a mechanical rotating shutter and each track was identified by a sequence of four dots. Since then, several strategies have made use of streaks and dots or their combinations in order to identify tracks and to solve the directional ambiguity of the particles' motion, typical of ME recordings (Adrian & Westerweel, 2011). Additionally, methods such as displacement biasing, image shifting, pulse tagging and colour coding have been implemented to recover the temporal direction information [Adrian 1986, Goss et al., 1989, Bertuccioli et al., 1996, Grant & Liu 1990, Landreth & Adrian 1988, Landreth et al., 2004]. With the development of high-speed imagers, double-exposure (DE) and ME techniques became unnecessary, as single exposure images of particle tracers could be recorded in rapid succession (Hain & Kaehler, 2007).

In more recent times, the development of efficient 3D particle tracking algorithms (e.g. Shake-The-Box, STB, Schanz et al., 2016) has extended the application of particle tracking to recordings with high seeding density. Yet, for the study of aerodynamic flow regimes with flow velocity in the order of 100 m/s, recording rates exceeding 10 kHz may be needed, which are not achievable with current hardware (Beresh et al., 2018). For large-scale experiments of industrial aerodynamics, dual frame PIV systems are commonly employed, where two pulses are recorded with a short time separation of the order of microseconds. Large-scale experiments employing helium-filled soap bubbles (HFSB) in wind tunnels (Scarano, et al., 2015) have been for instance recently conducted by Faleiros et al. (2021) to study of the flow in the wake of the propeller on a tilt-rotor aircraft.

Attempts to improve on the double-pulse strategy (in terms of dynamic velocity range DVR) require either multiple iterations on the selection of the time step  $\Delta t$  (multi- $\Delta t$  3D-PTV, Saredi et al., 2020) or adopting again multiple-exposure techniques (Novara et al. 2016). The latter authors have demonstrated the STB technique based on double-exposure recordings to investigate a high-speed jet at Mach 0.84 by (Manovski et al., 2021).

Experiments with HFSB in aerodynamic wind tunnels are often performed at a limited seeding density (typically  $\text{ppp} < 0.01$ ), which opens the opportunity to investigate recording techniques that involve more than two exposures in an image frame. Such approaches have been investigated in the early works cited above, but not recently, in combination with the capabilities of digital double-frame recording devices for PIV. A particular question arising for ME recordings is the arrangement of the sequence of pulses such that it results into a unique pattern easily recognized by a detection algorithm.

The present study investigates such approaches to the design of the time sequence for ME PTV recordings. We present first the concept. The recognition of the particle images belonging to the same trajectory is based on the specific time sequence of the laser pulses such that the scaled

particles positions in a track coincide with the laser pulse sequence at a unique condition of correspondence. The method is demonstrated for application with double-frame recordings, with a single-exposure first frame and a multi-exposure second frame.

The article opens with a description of the method working principle and the time sequence design is discussed in Section 3. An application of the two-frame method to the turbulent flow over a cylindrical obstacle is presented in Section 4.

## 2. Working principle of ME PTV

PTV recordings can be obtained nowadays in a number of modes, given the state-of-the-art of today's cameras:

- 1) single frame, single exposure, continuous (high speed cameras and lasers or LED);
- 2) double frame, single exposure (low repetition rate double frame cameras and lasers or LED);
- 3) single frame ME (low repetition rate single frame cameras, burst-mode or high-speed illumination);
- 4) double frame, ME in both frames (low repetition rate double frame cameras and high-speed or burst-mode illumination);
- 5) double frame, single exposure in the first frame and ME in the second frame (low repetition-rate cameras and high-speed or burst-mode illumination)

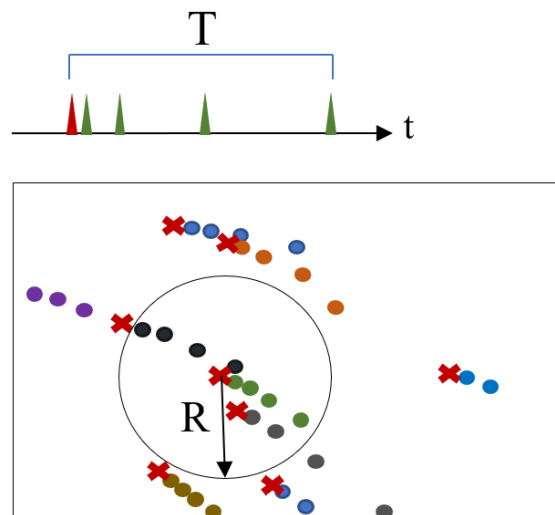


Fig 1 : Illumination timing sequence for case 5 (top); resulting particle tracks recorded (bottom). First exposure as a cross and following by dots, tracks distinct by color. Circular search region.

The discussion here will focus on the last configuration, whereby a single exposure of the tracers is recorded on a separate frame. A schematic description of the resulting images for 5 exposures in total is given in Figure 1, where the particle images of the first frame are represented by a cross and those of the second frame by dots. As a result, the tracers trajectory is sampled by a single position in the first frame and over a relatively long interval in the second frame.

The theory to design ME sampling sequences and analyze the resulting recordings is introduced here based on the following proposition: under nearly constant track velocity, there is a similarity (proportionality) between the time sequence of the illumination pulses and the cumulative distance travelled in space by the particle between these pulses. Such similarity can be exploited for trajectory identification and quantified by the inner-product operator.

Every particle recorded on the first frame represents the initial position a track. Around every such location, a circle in 2D (a sphere in 3D) is taken of radius  $R = V_{\text{ref}} \cdot T$ , where  $V_{\text{ref}}$  is a reference velocity and  $T$  is the total time elapsed in the illumination sequence. Inside this region, a number of approaches can be used to obtain candidate tracks with  $N$  exposures. Arguably, the simplest approach is a combinatorial generation of particle tracks. An example of two such tracks is shown in Figure 2 by orange and blue lines. From all the possible tracks generated this way, ideally only one will produce a similarity match, and that would be accepted as a track. The case in Figure 2 is that the combination corresponding to #1 is an incorrect one, and the one corresponding to #2 is the correct track. The track filtering is performed with similarity measures of the particle traveled distance to the reference illumination sequence in time, with operations elaborated in section 2.2.

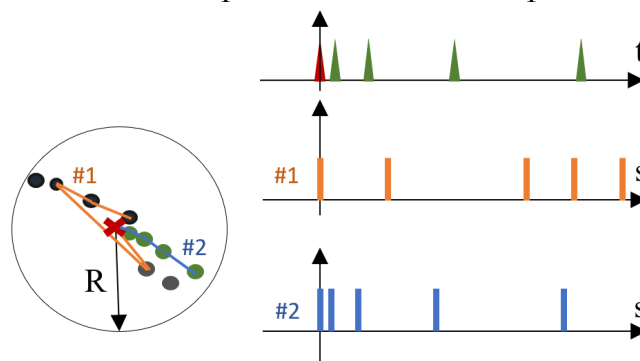


Fig 2 : Reference illumination timing sequence (top); the cumulative distance  $s$  covered by the particles in combinations #1 and #2 respectively (rows 2 and 3; right).

One relevant component of the multi-exposure image recording approach is the illumination time sequence. To clarify the preference for an irregular, or asymmetric, timing sequence, two of the major issues of the uniformly-spaced time sequence are discussed. The first is the directional

ambiguity and the second is a moderate ambiguity to the scaling operation. These concepts are qualitatively illustrated in Figure 3.

Here the tracer is recorded at times ranging from  $t_1$  to  $t_5$ . If the particle is illuminated at constant time intervals, the direction of its motion cannot be determined from the sole image recordings. Additionally, if one of the particles (e.g. the first one or the last one of the sequence) is not reconstructed, then a time-stamp cannot be assigned unequivocally to all the remaining particles. Conversely, a non-uniform sampling sequence (Figure 3-right) encodes the direction of motion. In fact, for a particle travelling at nearly constant velocity, the distance covered by the tracer will be proportional to the time intervals between the illumination pulses, thus solving the directional ambiguity.

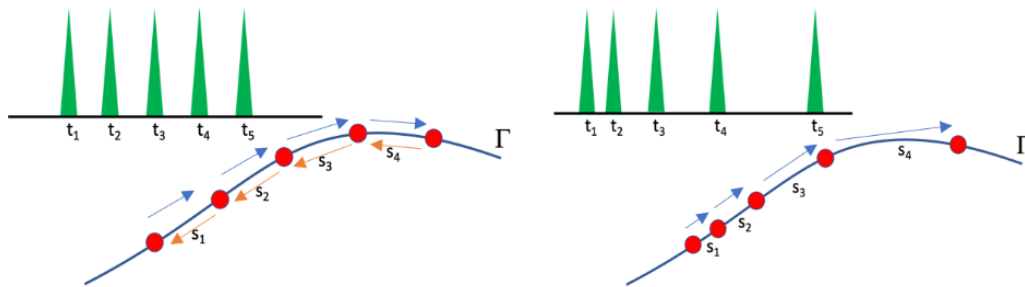


Fig 3 : Trajectory and its samples according to a sequence of regular (left) and irregular (right) illumination pulses.

The second requirement for such approach concerns the signal to noise ratio (SNR) of the scaling and inner product operation. For sake of illustration, we compare periodic and non-periodic signals, making an analogy to the well-known spatial cross-correlation analysis for PIV images.

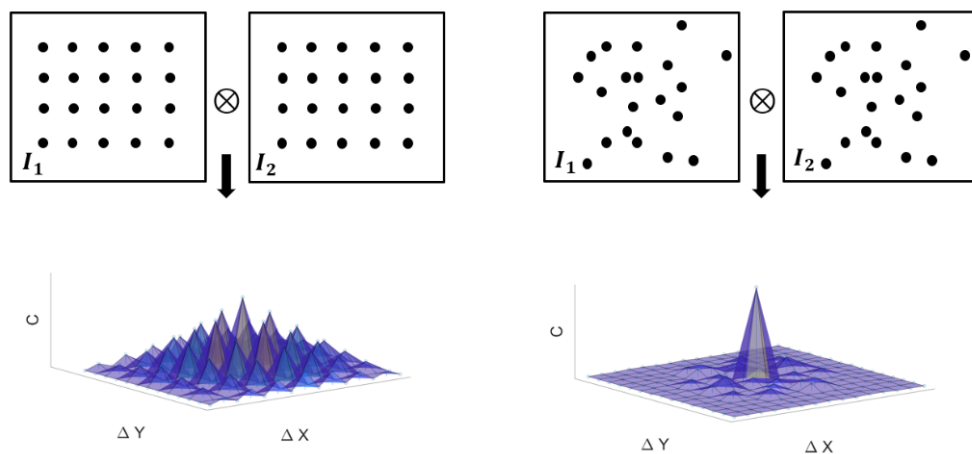


Fig 4 : Intensity map of hypothetical PIV recordings with regularly spaced tracer particles (top-left) and its autocorrelation map (bottom); same properties for randomly distributed particles (right).

Figure 4-left shows the auto-correlation  $C$  of regularly spaced particle images, whereas on the right the case with randomly distributed particles is illustrated. The irregularity of the latter distribution produces a unique condition for multiple matching (or pairing), giving rise to a correlation map with a distinct peak. In contrast, the correlation of the periodic signal yields multiple peaks of comparable heights, modulated with a triangular function. Based on the discussion above, the illumination time sequence shall be chosen such that the correlation analysis yields a distinct peak, clearly higher than any other spurious peak.

The next section introduces the variables and properties relevant to the quantitative analysis described qualitatively so far.

## 2.1 Nomenclature and definitions

A trajectory  $\Gamma$  is defined as the position  $\vec{r}$  of a tracer during a time interval  $T$ .

$$\Gamma: \vec{r}(\tau) \quad \tau \in T \quad (1)$$

A sampling time sequence vector is defined by a finite sequence of (illumination) pulses at  $n$  time instants:

$$\tau_{ref} = (\tau_1, \tau_2, \dots, \tau_n) \quad (2)$$

At the selected time instants, the particle assumes positions:

$$\vec{R} = (\vec{r}_1, \vec{r}_2, \dots, \vec{r}_n) \quad (3)$$

Based on the  $n$  selected time instants,  $n-1$  time intervals are defined in the sequence vector  $\Delta\tau$ :

$$\Delta\tau = (\tau_2 - \tau_1, \tau_3 - \tau_2, \dots, \tau_n - \tau_{n-1}) = (\tau_1, \tau_2, \dots, \tau_{n-1}) \quad (4)$$

and the Euclidian distance travelled during the time intervals is given as a vector  $\Delta s$ :

$$\Delta s = (|\vec{r}_2 - \vec{r}_1|, \dots, |\vec{r}_n - \vec{r}_{n-1}|) = (\Delta s_1, \Delta s_2, \dots, \Delta s_{n-1}) \quad (5)$$

Finally, the cumulative Euclidian distance travelled by a tracer is given by:

$$s = (\Delta s_1, \Delta s_1 + \Delta s_2, \dots, \sum_{i=1}^{n-1} \Delta s_i) = (s_1, \dots, s_{n-1}) \quad (6)$$

## 2.2 Time-Space similarity by homothety

Let us consider the case where the magnitude of the particle velocity  $|V|$  remains approximately constant during the observation time  $T$ . This velocity is not known a priori but the sequence pulse timing is known. Having selected a set of particle images, the scaling between their occurrence in space and the illumination pulses is done using a homothetic transformation of the 1D vector of pulses:

$$\tau_{c,j} = [s]/|V_j| \Big|_{j=1}^n \quad (7)$$

where  $c$  stands for 'candidate' sequence and  $n$  is the number of scaling velocities considered. A point in space is fixed, and eqn. (7) is applied around it. The fixed point is chosen here as the time of the first pulse in the first frame - and transforms each point in  $[s]$  to another point  $\tau$  that is scaled by a factor  $V$ . In the ideal case of constant velocity  $v_0$  along a track,  $[s/v_0]$  will coincide with  $[\tau]$ . The obtained sequences are modelled as Gaussian pulse trains. The Gaussian pulses are produced around the scaled position values. The amplitude of the pulses in the pulse train is set to 1, and the standard deviation can be decided based on the estimated particle position uncertainty.

The complete pulse sequence is modelled according to:

$$f(\tau) = \sum_{i=1}^N e^{-\frac{(\tau-\tau_i)^2}{2\sigma_f^2}} \quad (8)$$

where  $N$  is the number of pulses (exposures) and  $\sigma_f$  is the standard deviation of the temporal pulses.

$$g(\tau, V) = \sum_{i=1}^N e^{-\frac{(\tau-\frac{s_i}{V})^2}{2\sigma_g^2}} \quad (9)$$

where  $\sigma_g$  is the standard deviation of the scaled position pulses. For each velocity scaling value, the normalized inner product of  $G_{t\_track}$  and the reference time yields a value  $C$  as:

$$C(V) = \frac{(f \cdot g)}{(f \cdot f)} = \frac{\sum_k f(\tau_k)g(\tau_k, V)}{\sum_k f(\tau_k)f(\tau_k)} \quad (10)$$

where  $k$  runs over the length of the discretization. The result of plotting  $C$  vs. the range of estimated velocity values for the case of a valid track looks like the plot shown in Figure 5. This is the case for a synthetically generated track with 5 instances.

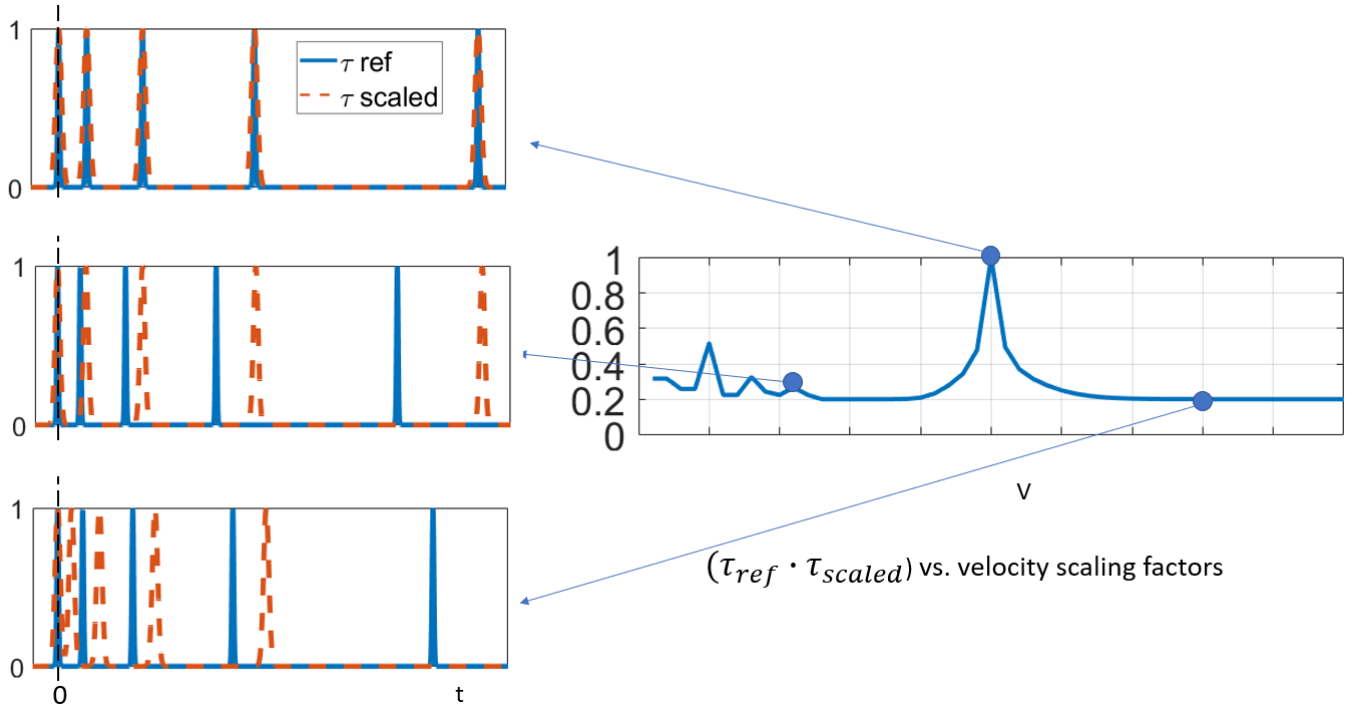


Fig 5 : Left: Plots of the candidate time sequences (in dashed lines) on top of the reference time signal for different scaling factors, scaled around position 0. Right: Map of the normalized inner product vs. the tested velocity scaling vectors to test track identity.

Note that at the peak C value, the correct scaling velocity will result in the maximum overlap between the reference and candidate sequence. If on the other hand the scaling velocity is too low, the signal is stretched, and if it too high, the signal is compressed, resulting in lower overlap in both cases.

The validity of the track is decided based on the value of  $C_{max}$  and SNR. After the track validity has been established, further analysis of refinements can be used to extract the track velocity, such as a refinement in the hypothesized velocity values discretization, refinements in the Gaussian width of the convolution, a polynomial fit to the track positions from which velocity and acceleration can be obtained, etc.

### 3. Time sequence design

The sampling time sequence shall be designed to optimize track identification reliability and DVR. The criterion used to differentiate between different options is the SNR. Typically the SNR is defined (Xue *et al.* 2014) as:

$$SNR = C_{max} / C_2 \quad (11)$$

However, because the homothety is centered around the first pulse, one pulse will always be coinciding between the reference and any scaled sequence. It can be noted from Figure 8 that the noise floor of the result of the operations is 0.2. More generally, if a pulse is chosen as the anchor,

the noise floor will be  $1/N$ . This situation can be avoided by choosing a different anchor point for the homothetic transformation, but it will not be discussed here. A different definition of the SNR which is more suitable to this case is:

$$\text{SNR} = \frac{(C_{max} - 1/N)}{(C_2 - 1/N)} \quad (12)$$

The goal is to have a sequence of time separations that minimizes other 'spurious' peaks due to parts of the scaled signal coinciding with parts of the reference. In order to investigate different options four different sequences of  $\Delta\tau$  are considered:

- uniform intervals

$$\Delta\tau = \text{const} \quad (13)$$

- arithmetic progression intervals

$$\Delta\tau_k = \Delta\tau_1 + (k - 1)d \quad (14)$$

where  $d$  is the (constant) difference between two consecutive  $\Delta\tau$  values.

- geometric progression intervals

$$\Delta\tau_k = a d^{k-1} \quad (15)$$

where  $a$  is a scale factor.

- incommensurable interval

$$\Delta\tau_n / \Delta\tau_{n-1} = \text{irrational} \quad (16)$$

The different time series generated using these intervals as well as the resulting dot product coefficients with the candidate time series are plotted in Figure 6. For these plots, a synthetically generated track was used for the sake of simplicity. The  $x$  are generated along a 20 ms interval with 0.5 ms discretization, and with a constant velocity of 5 m/s in the  $x$ -direction. Then, a ME sequence is generated with the different intervals outlined here. This spatial signal is scaled back to time, diving by a range of velocities 0-50 m/s, discretized by 0.5 m/s, according to the homothetic transformation outlined in Section 2.2.

The SNR as defined by eqn. (12) for each of the different series is reported in Table 1. The incommensurable time intervals give the largest SNR.

It can be added that the criteria mentioned here do not necessitate a monotonically increasing progression. For the case of double-frame recordings, it is preferred to have the smallest time separation first, or more specifically in the interframe, as that will increase the probability of correct first particle pairing. The longest time separation is preferred in the multiply exposed

frame such as to avoid particle overlap. The rest of the entries do not need to follow a specific order.

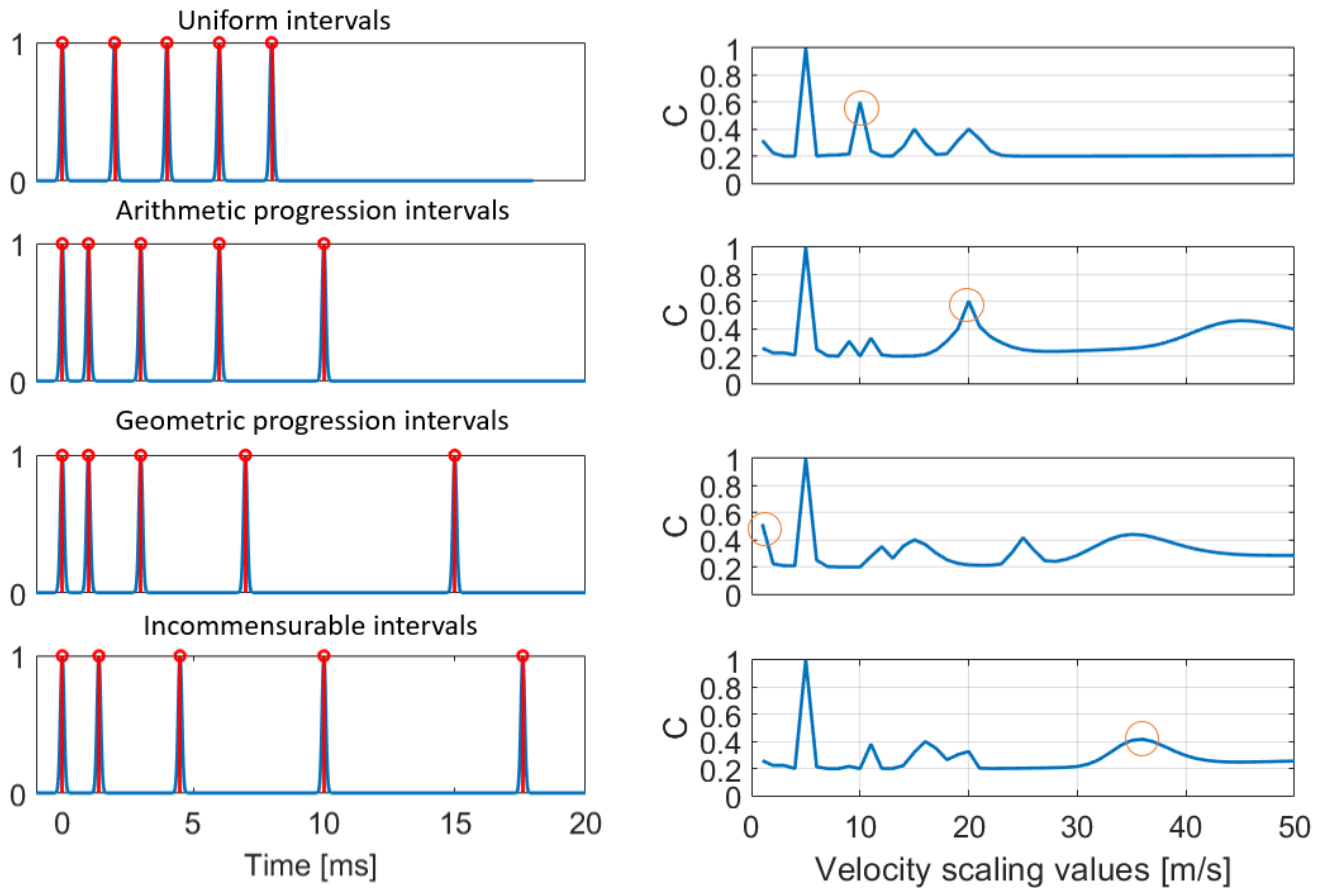


Fig 6: Left) The time sequences generated with the time intervals denoted on top of each plot. Right) The corresponding plot of the normalized inner product of the discretized signal for a range of scaling factors. The second highest peak of each inner-product function is highlighted with a red circle.

Time Intervals	SNR	
	N = 5	N = 10
Uniform : $\Delta\tau = [2\ 2\ 2\ 2]\ ms$	2	2.6
Arithmetic : $\Delta\tau = [1\ 2\ 3\ 4]\ ms$	2.1	2.7
Geometric : $\Delta\tau = [1\ 2\ 4\ 8]\ ms$	3.2	6.7
Incomm. $\Delta\tau = [\sqrt{2}, \pi, \sqrt{30}, \sqrt{58}]\ ms$	4	8

Table 1 : SNR values for different illumination time sequences

A number of criteria that are important to the time sequence design are:

- a sequence with regular pulse intervals suffers from directional ambiguity and low SNR, thus an irregularly spaced and asymmetric sequence is favored;
- the robustness of track identification depends upon the SNR of the inner product coefficient maps;
- what range of velocities needs to be considered, i.e. how accurately it can be considered to be known a priori, and for how long it remains constant;
- a minimum time separation needs to be defined that avoids overlapping of the images of the same particle;
- a maximum displacement resulting from the longest time interval can be defined.

For application to real experimental data, the SNR will also be subject to measurement noise, acceleration in tracks, overlapping particles, etc. In the next section, the application of the algorithm to the flow over a cylindrical obstacle is presented.

#### 4. Application to experimental data

The experiment was performed at the Aerodynamics Laboratory of the Aerospace Engineering Faculty of TU Delft. HFSB of  $\sim 300$  micron were used as flow tracers. An sCMOS camera with 4MPx resolution and a high speed laser (25 mJ/pulse at 1 kHz) were employed for the recording and illumination.

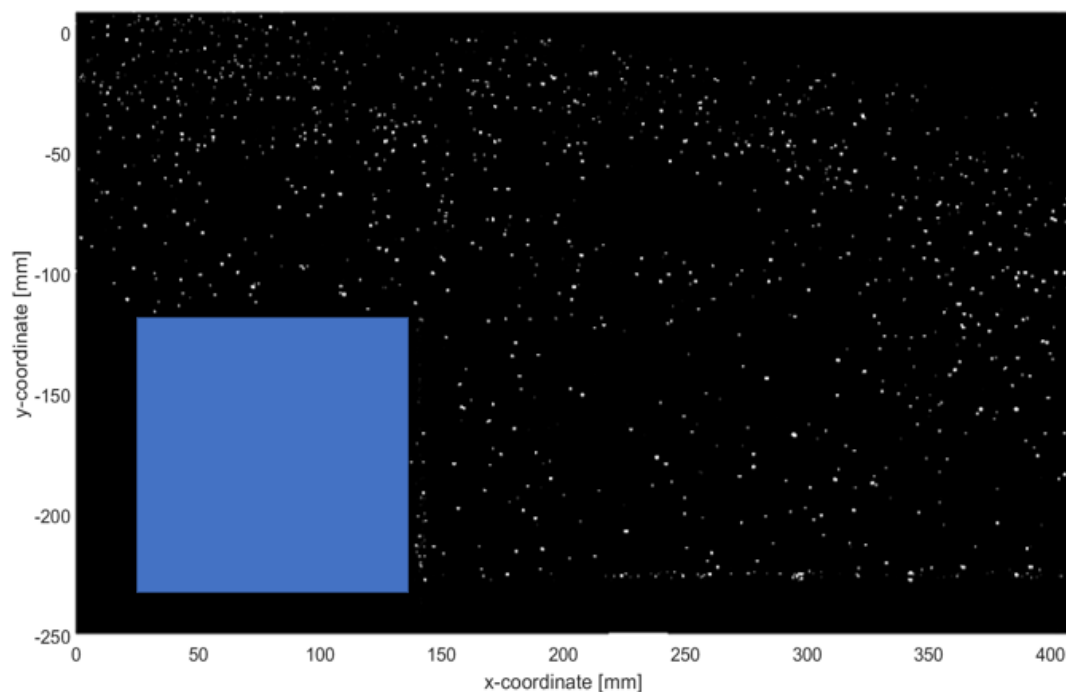


Fig 7: Example of an image from the recorded sequence. The first frame with a single exposure with the cylinder is shown in a blue box is represented. The contrast of the image has been improved to make the particles more easily visible.

The planar PIV measurements were performed with freestream velocity of  $\sim 5\text{m/s}$  and at recording frequency 5 kHz using the LaVision Davis 10.1.2 software. The measurement plane was located across the center line with 1 cm of thickness. The ppp of the images is  $\sim 0.004$ ; conventional 2D PTV was used as ground truth for comparison with the ME method. The ME images have been simulated for the case of double-frame recordings by importing the particle fields in one exposure in the first frame, and adding the particle fields from multiple exposures in the second (so the ppp in the second frame goes up to  $\sim 0.02$ ). The time sampling interval used to simulate the multiple exposures is :  $\Delta\tau = [1, \pi i, \sqrt{30}, \sqrt{58}] * 0.2\text{ms}$ , where the first interval is interframe. These values were rounded to the nearest  $\Delta\tau$  value that was available from the time resolved recording.

In the ME mode, the tracking is initiated with a nearest neighbor search in the interframe, as the time interval chosen there is small enough such that the particle displacement is smaller than the mean inter-particle distance. This velocity estimator  $V_0$  can be used to limit the search region for the full track as denoted by the dotted lines in Figure 6, in the closeup region. Here it can be seen how starting from the first instance of a track (known from frame 1), a circle of radius  $R = V_0 * T$  is constructed. If there were no other information available, one would have to try all the combinations consisting of 5 particles within this region with the beginning of the track known. However, with the double frame recording information of the first pairing, one can use the direction and magnitude of the velocity obtained from the first pair to construct a baseline for the future search. In this way, the circle can be reduced to a triangle, or in 3D the sphere into a cone. The angle of the area around the direction of  $V_0$  can be chosen to allow for acceleration. In Figure 6 in the close-up region, in black is shown the correct solution and in red a number of incorrect candidates. Their scaling and inner product results are shown in the bottom row of the figure. This is an example to demonstrate the effectiveness of the method to differentiate a valid track in experimental data.

The method is successful for unambiguously detection of more than 75% of the tracks in this way, as indicated by the SNR color coded tracks in Figure 7. The majority of the tracks have an SNR of above 2. Around 5% of the tracks have SNR  $\sim 0$  which is coming from the fact that  $C_{\text{max}}$  is almost zero. A visual inspection of the data identifies these tracks as stagnant, that is all the instances of the particle overlap on top of each other so the similarity measure fails there. There is  $\sim 10\%$  of the tracks where the SNR is between 1.3 and 2 which could be considered to be somewhat ambiguous in a first pass. This appears to be the case on tracks of moderate curvature due to acceleration. Further data analysis is needed for quantification of these effects.

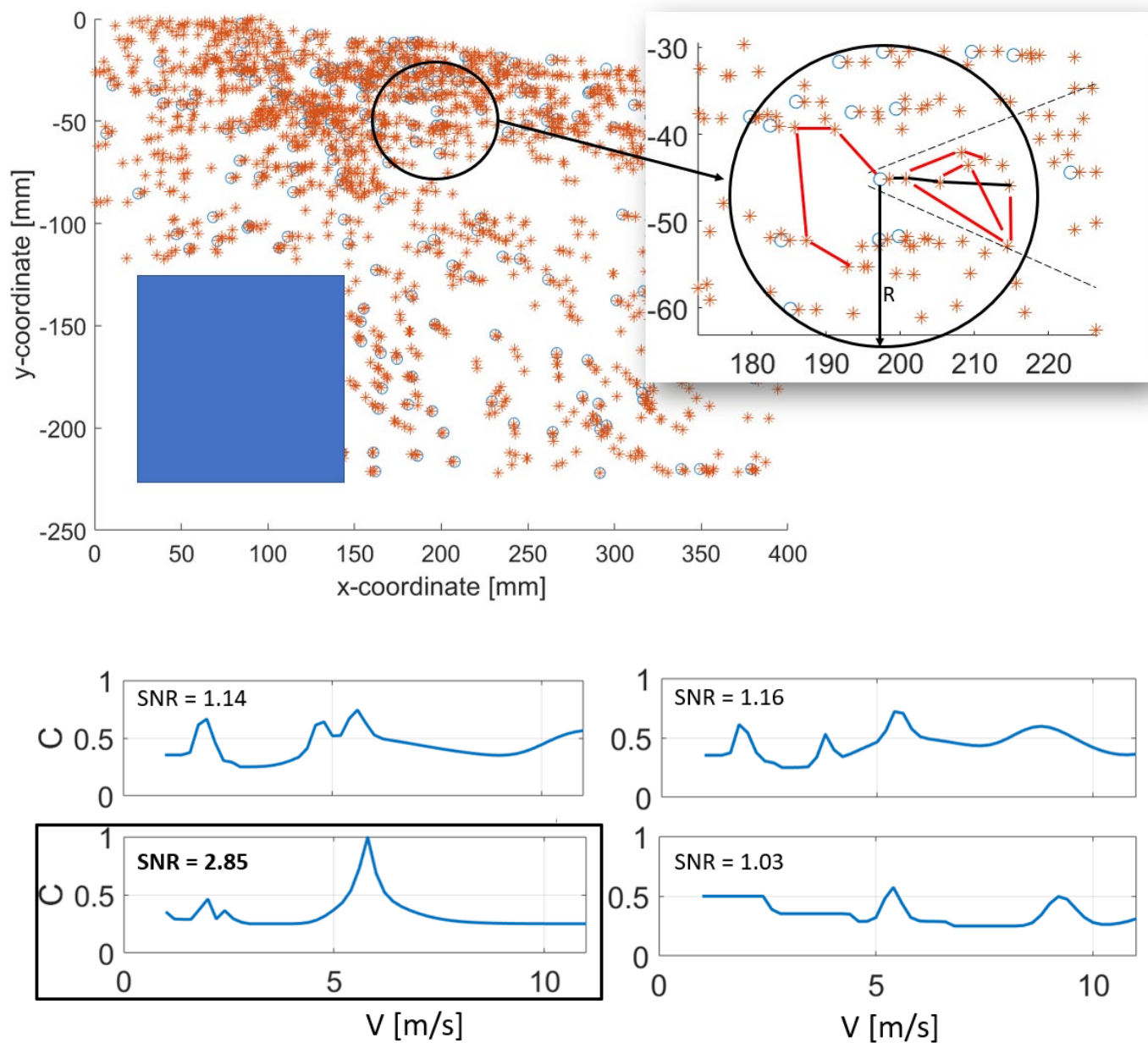


Fig 5 : Top: The multiply exposed images resulting from 5 exposures (first exposure in a blue circle, the rest in red asterisks). Bottom: The inner product plots of tracks obtained by different combinations of particles inside the outlined circle region. The valid track combination is outlined in the black box.

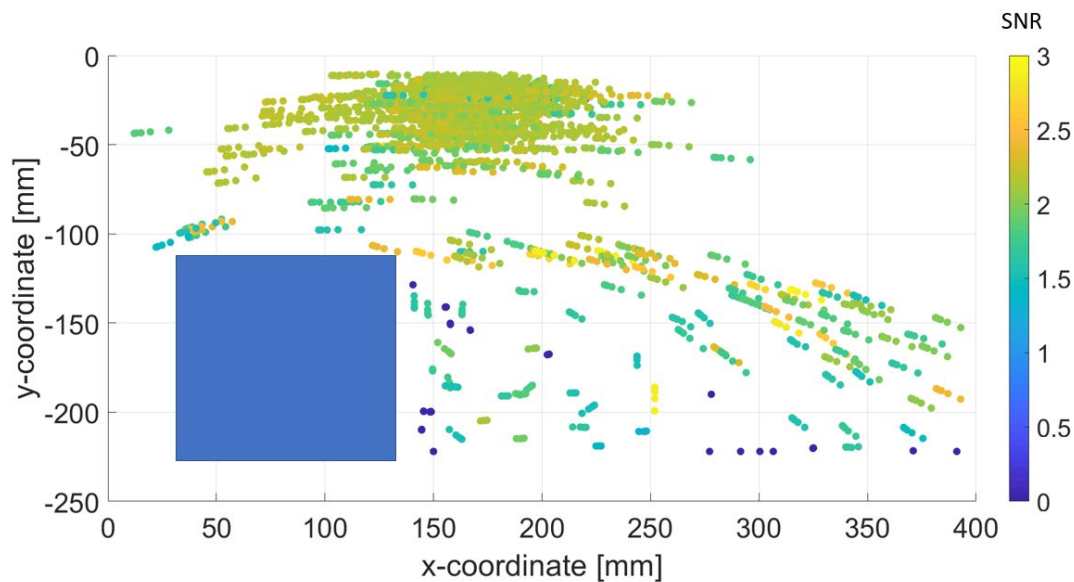


Figure 6 : Approx. 500 ME tracks are shown color coded by the SNR.

## 6. Conclusion

A method for track identification in multi-pulse, multi-exposure recordings is introduced for potential application in high-speed flow measurements with low speed cameras. The methods reliance on low seeding density makes it suitable for large-scale measurements with HFSB.

The method uses a combination of homothetic scaling and inner product operator for trajectory identification. It is based on the similarity between the time sequence of multiple pulses and the array of positions along the trajectory of a Lagrangian tracer. The properties of the multi-pulse sampling time sequence are discussed in terms of the resulting SNR.

The concept is demonstrated on simulated multiple exposure images from a real experimental dataset of the flow across a cylinder obstacle. The results show that the method detects tracks successfully in the nearly constant velocity regions of the domain, and is also reliable for tracks with moderate acceleration. The very low velocity regions where the particle overlaps over several exposures deteriorates detection.

Future work is foreseen for the acquisition of experimental datasets with the multiple-exposure recording technique and high velocity application with HFSB, to further assess the potential and limitations of the technique.

## Acknowledgements

The authors would like to acknowledge the work of Edoardo Saredi for the acquisition of the experimental dataset.

## References

- Adrian, R. (1986). Image shifting technique to resolve directional ambiguity in double-pulsed velocimetry. *Appl. Opt.* 25(21), 3855-3858.
- Adrian, R. (1991). Particle-imaging techniques for experimental fluid mechanics. *Annu. Rev. Fluid Mech.* 23 (1), 261-304.
- Adrian, R., & Westerweel, J. (2011). *Particle Image Velocimetry*. Cambridge University Press.
- Bertuccioli, L., Gopalan, S., & Katz, J. (1996). Image shifting for PIV using birefringement and ferroelectric liquid crystals . *Exp. Fluids* 21(5), 341-346.
- Faleiros, D. (2021). *Soap bubbles for large-scale PIV: Generation, control and tracing accuracy*.
- Goss, L., Post, M., Trump, D., & Sarka, B. (1989). Two-color particle velocimetry. *Laser Institute of America*, (pp. 101-111).
- Grant, I., & Liu, A. (1990). Directional ambiguity resolution in particle image velocimetry by pulse tagging. *Exp. Fluids* 10(2-3), 71-76.
- Hain, R., & Kaehler, C. (2007). Fundamentals of multiframe particle image velocimetry. *Exp. Fluids* 42:575-587.
- Landreth, C., & Adrian, R. (1988). Electrooptical image shifting for particle image velocimetry. *Appl. Opt.* 27(20), 4216-4220.
- Landreth, C., Adrian, R., & Yao, C. (2004). Double pulsed particle image velocimeter with directional resolution for complex flows. *Exp. Fluids* 6(2), 119-128.
- Lynch, K., & Scarano, F. (2013). A high-order time-accurate interrogation method for time-resolved PIV. *Meas. Sci. Technol.* 24, 16.
- Lynch, K., & Scarano, F. (2014). Material acceleration estimation by four-pulse tomo-PIV. *Meas. Sci. Technol* 25:084005.
- Manovski, P., Novara, M., Mohan, N., Geisler, R., Schanz, D., Agocs, J., . . . Schroeder, A. (2021). 3D Lagrangian particle tracking of a subsonic jet using multi-pulse Shake-The-Box. *Experimental Thermal and Fluid Science*.
- Novara, M., Schanz, D., Gesemann, S., Lynch, K., & Schroeder, A. (2016). Lagrangian 3D particle tracking for multi-pulse systems: performance assessment and application of Shake-The-Box. *18th international symposium on application of laser techniques to fluid mechanics*. Lisbon, Portugal.
- Novara, M., Schanz, D., Reuther, N., Kaehler, C., & Schroeder, A. (2016). Lagrangian 3D particle tracking in high-speed flows: Shake-The-Box for multi-pulse systems. *Exp. Fluids* 57(128).
- Saredi, E., Sciacchitano, A., & Scarano, F. (2020). Multi-dt 3D-PTV based on Reynolds decomposition. *Meas. Sci. Technol.* 31, 15.
- Scarano, F., Ghaemi, S., Caridi, G., Bosbach, J., Dierksheide, U., & Sciacchitano, A. (2015). On the use of helium-filled soap bubbles for large-scale tomographic PIV in wind tunnel experiments. *Exp. Fluids* 56(42).
- Schanz, D., Gesemann, S., & Schroeder, A. (2016). Shake-The-Box: Lagrangian particle tracking at high particle image densities. *Exp. Fluids* 57(9).

- Sciacchitano, A., Scarano, F., & Wieneke, B. (2012). Multi-frame pyramid correlation for time-resolved PIV. *Exp. Fluids* 53, 1087-1105.
- Souverein, L., van Oudheusden, B., Scarano, F., & Dupont, P. (2009). Application of dual-plane particle image velocimetry (dual-PIV) technique for the unsteadiness characterization of a shock wave turbulent boundary layer interaction. *Meas. Sci. Technol* 20: 074003.
- Utami, T., & Ueno, T. (1984). Visualization and picture processing of turbulent flow. *Exp. Fluids* 2, 25-32.